Chinese Chemical Letters 37 (2026) 111087

Contents lists available at ScienceDirect

Chinese Chemical Letters

journal homepage: www.elsevier.com/locate/cclet

Integrated implantable triboelectric charge collector for nerve repair

Chenglong Cai[a,1], Ting Wang[a,1,*], Yixin Zhang[a], Conghao Lin[a], Zhangqi Feng[b], Yan Cai[a,*], Nongyue He[a]

[a] State Key Laboratory of Digital Medical Engineering, Jiangsu Key Laboratory for Biomaterials and Devices, School of Biological Science and Medical Engineering, Southeast University, Nanjing 210096, China
[b] School of Chemistry and Chemical Engineering, Nanjing University of Science and Technology, Nanjing 210094, China

ARTICLE INFO

Article history:
Received 24 November 2024
Revised 6 March 2025
Accepted 12 March 2025
Available online 13 March 2025

Keywords:
Triboelectric nanogenerator
Nerve repair
Electrical stimulation
Implantable flexible devices
Mesoporous material

ABSTRACT

The employment of low-frequency electrical stimulation therapy has been shown to elicit a pronounced depolarization of neurons, thereby initiating the regenerative signaling cascades within neural cells, which is favorable for the regeneration of neural cells. In this study, we designed the flexible triboelectric nanogenerator device (TENG) to treat injury of peripheral nerve, which is combined with mesoporous silica (H-SiO_2), high dielectric performance of polydimethylsiloxane (PDMS), and connected to biocompatible and conductive polycaprolactone (PCL) conduit materials for limited power generation to neurobioelectric response adaptation. By adjusting the content of H-SiO_2 and the amount of PDMS monomers, the electrical performance of the device is optimized. Through the charge collection effect of silica molecular sieve, the endogenous neural electric field in nerve injury was stabilized, ensuring the consistency of the electrical stimulation level that is crucial for maintaining resting membrane potential. *In vitro* experiments clearly demonstrated that electrical stimulation derived from the triboelectric nanogenerator significantly promotes cell proliferation. Further animal experiments confirmed that electrical stimulation can effectively treat sciatic nerve injury and accelerate axonal regeneration. Based on experimental outcomes, we have developed an implantable sciatic nerve system that can stably generate effective electrical pulses in response to rat movement through charge collection. This system regulates the electric field around the injured sciatic nerve, maintains the electric field threshold required for rapid nerve tissue repair, and accelerates the recovery of nerve function.

© 2025 Published by Elsevier B.V. on behalf of Chinese Chemical Society and Institute of Materia Medica, Chinese Academy of Medical Sciences.

Peripheral nerve injury, as a hub for transmitting sensory signals, once damaged, can bring significant economic and social burdens to patients, families, and society [1]. It is estimated that approximately 2%–3% of primary trauma patients have peripheral nerve damage, and 25% of patients are unable to return to work within 1.5 years after surgery [2,3]. With the continuous improvement of medical technology, various treatment methods for nerve repair are emerging, but clinical treatment is still not satisfactory. There is an urgent need for an effective and long-term stimulating treatment to promote peripheral nerve repair.

The essence of peripheral nerve injury is the degeneration of Wallerian fibers in the distal nerve stump, leading to the atrophy of Schwann cells and the inability to provide axonal regeneration. Electrical stimulation therapy, as a treatment method, can promote the growth and extension of neural processes by stimulating Schwann cells to secrete nerve growth factors [4–8]. Unlike physical or chemical interventions, the biological response to electrical stimulation in the nervous system is mediated through bioelectrical signaling mechanisms, such as intracellular Ca^{2+} waves and membrane potential changes, which promote neural growth [9,10]. Recent studies have demonstrated that electrical stimulation can activate the expression of key receptor proteins, including tropomyosin receptor kinase B (TrkB) receptor and phosphokinase A (PKA), and induce the upregulation of neurotrophic factors such as brain-derived neurotrophic factor (BDNF), nerve growth factor (NGF), and ciliary neurotrophic factor (CNTF). These factors create a conducive microenvironment for axonal regeneration, underscoring the potential of electrical stimulation as a therapeutic modality in neural repair [11–13].

In clinical practice, electrical stimulation is usually used as a recovery measure during and after surgery. For example, Al-Majed *et al.* employed an implantable electrical stimulator to facilitate the repair of facial neurons and enhance the content of neuronal cytoskeletal proteins [10]. Their findings indicated that optimal

* Corresponding authors.
E-mail addresses: tingwang@seu.edu.cn (T. Wang), yancai@seu.edu.cn (Y. Cai).
[1] These authors contributed equally to this work.

https://doi.org/10.1016/j.cclet.2025.111087
1001-8417/© 2025 Published by Elsevier B.V. on behalf of Chinese Chemical Society and Institute of Materia Medica, Chinese Academy of Medical Sciences.

repair efficacy was achieved at a stimulation frequency of 20 Hz [14–17]. Furthermore, Gordon *et al.* applied an electrical stimulator operating at a frequency of 20 Hz to alleviate symptoms associated with carpal tunnel syndrome and to expedite postoperative recovery during surgical procedures [18,19]. Although electrical stimulation is widely recognized for its therapeutic potential in the treatment of nerve damage, current commercial devices are hindered by their bulky design and limited cost-effectiveness, making it difficult to promote them on a large scale [20]. The emergence of self-powered nerve repair technology, which combines triboelectric nanogenerators with nerve scaffolds, offers a promising avenue for the development of implantable and flexible devices. For instance, devices made from triboelectric materials can generate electrical signals through mechanical vibrations, thereby altering neuronal membrane potentials, activating voltage-gated Ca^{2+} channels, and upregulating gene expression related to repair [21]. These actions collectively enhance cytoskeletal assembly, stimulate axonal sprouting, initiate cellular regeneration mechanisms, and ultimately promote axonal growth [22]. Although self-powered devices can provide a certain voltage to promote nerve cell growth, the placement of self-powered devices and variations in external motion patterns and forces make it difficult to provide a long-term stable power supply, resulting in irregular local discharge and an inability to provide a stable endogenous electric field for nerve tissue repair [23]. Therefore, how to maintain the stability of the voltage field strength in nerve tissue injury through engineering methods is one of the current research directions for self-powered devices [24–26].

Here, we present a triboelectric nanogenerator (TENG) device fabricated from mesoporous H-SiO_2 and polydimethylsiloxane (PDMS) monomers. Leveraging the intrinsic contact electrification properties of PDMS and metals, the charge density of the material can be rapidly enhanced. Concurrently, under conditions of high charge density and significant charge concentration gradients, charges that diffuse internally are captured and maintained by the H-SiO_2, thereby increasing the overall charge density of the triboelectric nanogenerator. The device, when integrated with a conductive polycaprolactone film embedded with silver nanoparticles (PCL-Ag), constitutes a self-powered neural scaffold capable of establishing a short-time stable electric field at the injury site. This novel configuration was employed to enhance the proliferation of PC12 nerve cells through mechanical stimulation, indicative of its potential to foster neural regeneration. The embedded and uniformly dispersed silica molecular sieve effectively collected the charge, maintain the stability of the voltage field strength in nerve tissue injury. Furthermore, when the device was implanted into rats, it leveraged the mechanical vibrations generated by the animals' natural movement to produce electrical current, thereby stimulating sciatic nerve repair. Our findings demonstrate that this integrated device is effective in facilitating the regeneration of the sciatic nerve, highlighting its innovative application in the field of neural engineering.

The preparation methods for H-SiO_2 nanoparticles and the triboelectric nanogenerator (TENG) device, as well as their physicochemical property characterizations are provided in the supporting information. Additionally, the *in vitro* and *in vivo* tests, including biocompatibility assays, nerve cell proliferation promotion experiments, and sciatic nerve repair experiments in animals, are documented in the supporting literature. Detailed experimental procedures for these tests are also supplied in the supporting information.

In the present investigation, we have enhanced the efficacy of TENG for applications within biological tissues. This was achieved by meticulously adjusting the voltage output generated by PDMS, facilitated by the incorporation of a specific ratio of mesoporous silica. The optimization of this composite material's formulation has resulted in a controlled modulation of the triboelectric effect, thereby augmenting the performance of the nanogenerators in harnessing mechanical energy from biological systems. As an excellent energy storage material, mesoporous silicon has been applied in energy storage and drug loading. For triboelectric nanogenerator, surface triboelectric changes easily dissipate in the air, especially after contact electrification ceases. Here, we propose the using of equidistributional mesoporous SiO_2 with a large specific surface area as effective bulk charge storage sites within PDMS to enhance the output performance of the TENG.

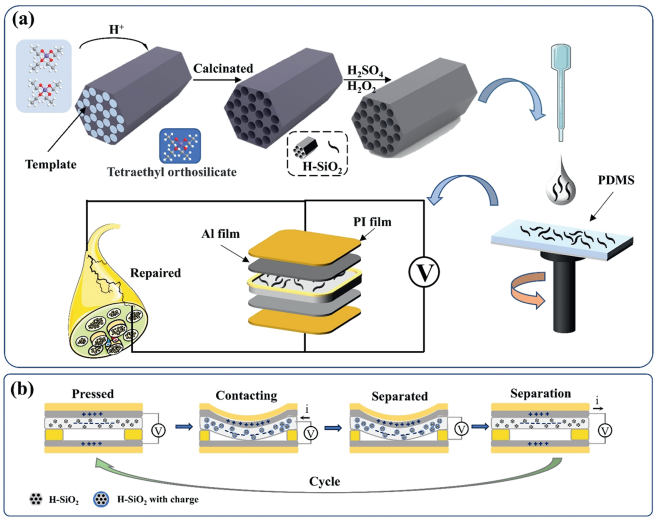


Fig. 1. (a) The schematic of triboelectric nanogenerator preparation, Tetraethyl orthosilicate was transformed into mesoporous silicon dioxide (H-SiO_2) through a template-assisted calcination process. Following this, a film was deposited *via* a rotary coating technique, and the components were subsequently integrated to fabricate a triboelectric nanogenerator. (b) The principles of electric signal generation of triboelectric nanogenerator, in the process of contact and separation.

Fig. 1a shows simply that the process of the design device, which is divided into three steps. First, we synthesized mesoporous H-SiO_2 with numerous oxygen-containing functional groups on its surface through calcination and oxidation treatment. Then the PDMS dielectric film with mesoporous H-SiO_2 is prepared by spinning-coating on a glass slide after mixing PDMS and H-SiO_2 particles. Finally, assemble it into a TENG device. Besides, in Fig. 1a, we also presented the internal structure diagram of the device. The polyimide tapes (PI) acts as insulation and protect the internal PDMS hybrid film. As charge transfer layers, the second layer and the fourth layer can realize free charge transfer and generate current; The PDMS&H-SiO_2 acts dielectric layer and separate with aluminum foil to transfer charge. Finally, combining the above layers.

Fig. 1b schematically illustrates the operational mechanism of the device, encompassing the processes of contact, separation, charge redistribution, and charge transformation. In the absence of contact between the two materials, no charge transfer occurs [27,28]. Upon the application of an external force to the TENG, the PDMS film comes into contact with the aluminum foil. At this juncture, due to PDMS's electron affinity, electrons are transferred from the aluminum foil to the PDMS surface, resulting in the conductive fabric acquiring a positive charge and the PDMS a negative charge. Concurrently, a portion of the charge generated by the PDMS is stored within the mesoporous silicon, augmenting the charge carried by the PDMS film and increasing the potential difference between the PDMS film and the metal. To maintain electrical neutrality, charge transfer occurs *via* an external wire, manifesting as a voltage signal on the voltmeter. Upon the removal of the external force, the PDMS film separates from the aluminum foil,

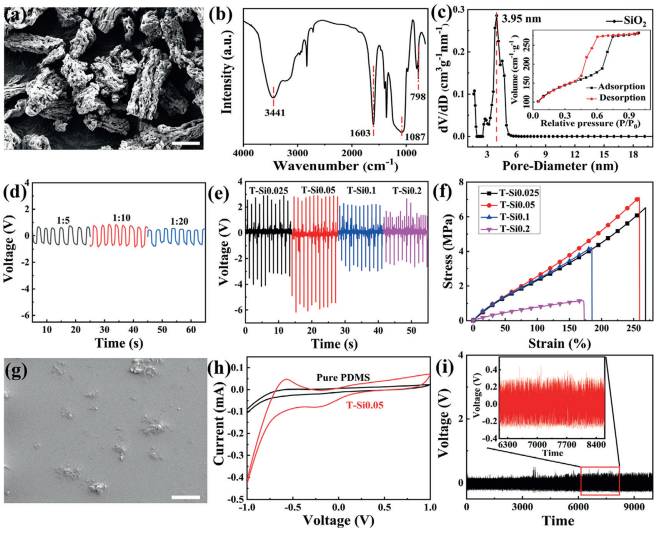


Fig. 2. Characterization of the properties of synthesized mesoporous H-SiO_2 and composite film. (a) The SEM of microporous H-SiO_2 nanoparticle. Scale bar: 10 μm. (b) The FT-IR of microporous H-SiO_2. (c) The pore size distribution and the adsorption isotherm curve of microporous H-SiO_2. (d) The output voltage of the PDMS with different monomer ratios. (e) The output voltage of the PDMS with different H-SiO_2 ratios. (f) The stress-strain curves of mixing with different H-SiO_2 ratios. (g) The SEM of mixing H-SiO_2 and PDMS. Scale bar: 2 μm. (h) The cyclic Voltammogram of pure PDMS and T-Si0.05 test in the three-electrode system. (i) The cycle-life of T-Si0.05 (F = 1 N).

disrupting the previous electrical neutrality. To reestablish charge balance, negative charges are transferred from the external circuit's aluminum foil to the PDMS film, once again registering a voltage signal on the voltmeter. Since a portion of the charge remains within the mesoporous silicon, the TENG continues to discharge and sustains the local voltage even after separation.

As shown in Fig. 2a, the morphology of the mesoporous H-SiO_2 demonstrates a cylindrical porous structure. We speculated that its pores grew along the Z-axis, indicating that the templates (Pluronic P123) were arranged in an orderly manner in the synthesis process, and tetraethyl orthosilicate gradually surrounded it until completely wrapped. Then, the internal template was continuously degraded through high-temperature calcination resulted to mesoporous silica material. The large specific surface area of mesoporous H-SiO_2 can better combine with PDMS monomers, which is conducive to further improving the overall mechanical strength of the membrane. Further, the functional groups of mesoporous H-SiO_2 with hydroxyl are explored by Fourier transform infrared spectrometer (FT-IR), as shown in Fig. 2b. The peaks corresponding to the symmetrical stretching vibration of the Si-O and asymmetric Si-O-Si stretching appeared at 798 and 1087 cm^{-1} [29,30]. The peaks at 3441, 984 and 1603 cm^{-1} were characteristic of the stretch vibration of the -OH bending in H_2O, Si-OH bending vibration and -OH bending. These results indicate that the as-prepared particle is microporous H-SiO_2 with many hydroxyl groups [31,32]. Fig. 2c shows the result of the H-SiO_2 pore size distribution. The H-SiO_2 sample presented a specific surface area of 482.286 m^2/g and an average pore size of 3.96 nm. The result of the N_2 adsorption/desorption isotherms was presented in the built-in small in Fig. 2c. H-SiO_2 had an appearance of type IV isotherm referred by classification of Brunauer-Emmett-Teller (BET) and exhibits a clear H_3 hysteresis loop, which illustrates the presence of a mesoporous structure with huge specific surface area.

In addition, we found during the testing process that the electrical properties of PDMS composite films are related to monomers and curing agents. Here we select different ratios of monomers and curing agents to test their output voltage. Fig. 2d shows the relationship between voltage and different ratios of curing agents and monomers. When the ratio of curing agent to monomer is 1:10 with the applied 40 N, we can see that it has the highest voltage output about 1.6 V, which illustrated the sensitivity of sensors is highest at this ratio. There may be a certain optimal value for the curing agent and monomer ratio to obtain highest voltage output. In PDMS film, the excessive monomer content leads to increase viscosity of film viscidity, which in turn reduces

The membrane's resilience and voltage output. But with the curing agent increasing, the output voltage also is decrease. Although the negative surface charge formed by PDMS is not related to its monomer and curing agent, it is related to its friction performance and flexibility [33–35]. Therefore, we chose a PDMS membrane with a curing agent and monomer ratio of 1:10 as the object of our further research. After determining the ratio of monomers and curing agents, we added H-SiO_2 with different contents to observe the morphology of the material and test its physical properties.

We prepared PDMS film with different H-SiO_2 content to test voltage output under a force of 40 N (T-SiX where X represents the content of mesoporous silica), as shown in Fig. 2e. It can be seen that under the same force, the output voltage has a maximum value about 8 V. When the content of mesoporous silicon increases to 0.2 g, the output potential difference is only about 4 V. The reason for this phenomenon may be that the suitable H-SiO_2 can increase the triboelectric characteristics of PDMS film. The scholarly literature has highlighted that mesoporous H-SiO_2, characterized by its substantial specific surface area, functions as an efficient charge reservoir within triboelectric nanogenerator is attributed to its capacity to harbor a greater number of charges, thereby enhancing the output performance of TENG [36,37]. However, the excess of hydrophilic mesoporous H-SiO_2 increasing the hydrophilic of TENG's surface, facilitating the formation of an adsorbed water layer. this hydration layer escalates the surface conductivity, which can precipitate surface discharge and consequently diminish the charge transfer capacity [38]. Fig. 2f shows the mechanical characteristics PDMS with different contents of SiO_2. The stress-strain curves of all samples show that the material breaks in the elastic stage without yield, so it belongs to brittle material. Brittle material, due to their impact sensitivity, can convert minor mechanical energy into electrical energy, which is beneficial for triboelectric nanogenerators to collect mechanical signals. Besides, due to the characteristic of muscles having a relatively high Young's modulus (∼100 kPa to ∼1 MPa), the triboelectric nanogenerator with a T-Si0.05 ratio has a Young's modulus consistent with that of muscles, thus matching the strength of muscles in motion. The reason for this phenomenon is that while PDMS is formed, the oxygen atoms in the molecular chain can form hydrogen bonds with -OH on the surface of mesoporous silicon, increasing PDMS's tensile strength. However, when excessive mesoporous silicon is doped into PDMS, a large number of mesoporous silicon agglomerates are due to uneven dispersion, resulting in many defects. Therefore, the tensile strength decreases with the increase of mesoporous silicon content. According to Figs. 2e and f, we selected PDMS called T-Si 0.05 as the membrane for our final device. Fig. 2g shows a scanning electron microscopy (SEM) image of the membrane T-Si0.05, with protrusions of varying sizes on the surface and mainly mesoporous H-SiO_2 inside. We intuitively observe that mesoporous H-SiO_2 mainly plays a role in increasing the contact area of PDMS, so it can be supposition that the overall charge transfer ability of the film will be improved.

The charge storage capacity of the films was assessed using cyclic voltammetry. We immersed a PDMS composite membrane, uniform in thickness and area (approximately 10 mm^2), into a phosphate buffered saline (PBS) solution with an applied window voltage of 2 V, as depicted in Fig. 2h. The results indicate that the

PDMS composite containing mesoporous silicon is capable of retaining a higher charge density. This enhanced charge retention is advantageous for establishing a more persistent local electric field at the site of nerve injury, thereby maintaining voltage stability and facilitating nerve repair. To elucidate the relationship between output voltage and applied force, which is crucial for evaluating the sensitivity and charge generation capability of our triboelectric nanogenerator, we conducted tests under varying pressures, as presented in Fig. S2 (Supporting information). A linear correlation between force and output voltage was observed, with an R^2 value of 0.99284. This regression analysis provides essential data support for the device's design and implantation within biological systems. Notably, rat muscle tissue typically exerts a force not exceeding 1 N during physical activity.

To ascertain the device's durability for *in vivo* simulation in Sprague-Dawley rats, we subjected it to 10,000 cycles of a 1 N force, and it maintained excellent voltage output performance, demonstrating its outstanding robustness. Animal experiments were approved by the Institutional Animal Care and Use Committee of Southeast University (No. 20240415051). The SEM image of PDMS with H-SiO_2 after 10,000 cycles also support robustness of triboelectric nanogenerator, as shown in Fig. S3 (Supporting information) [39,40]. In terms of flexibility, to demonstrate this characteristic more intuitively, a generator measuring approximately 10×10 mm was affixed to the thumb, as shown in Figs. S4a–c (Supporting information). It exhibited a significant degree of flexibility and was capable of generating a voltage of approximately 0.2 mV under flexed conditions, as illustrated in Fig. S4d (Supporting information). Collectively, these intrinsic properties indicate that the device possesses commendable charge storage ability, frictional power generation capability, flexibility, and robustness, rendering it suitable for prolonged and effective use within biological organisms.

In order to evaluate the electrical stimulation influence for PC12 cell, cell scratch experiment and cell cycle analysis *in vitro* experiment were carried out. The experimental schematic diagram is shown in Fig. 3a, PC12 neurons cell was extracted from young rats and subjected to electrical stimulation on the culture medium. To assessed the proliferation rate of cells under the influence of electrical stimulation, cell cycle assay kit and fluorescence intensity were used. As shown in Fig. 3b, we investigated the effect of electrical stimulation on cell proliferation through cell cycle dynamics research at 24, 48, and 72 h respectively. At 24 h, under the influence of electrical stimulation, we observed a shortening of the G1 and G2 phases of cells, indicating that the cells were striving to divide. However, in order to ensure successful division, the cells used more time to prepare, resulting in an extension of the S phase, indicating an accelerated growth rate [41,42]. At 48 h, shortening of G1 and S phases indicates that certain stages of the cell cycle are accelerated, while the extension of G2 phase means that cells need more time to prepare or repair before entering mitosis (M phase). This suggests that under the influence of electrical stimulation, the rate of cell proliferation increases, but as a result, the maturity of cells decreases, leading to a longer preparation time for cell division, manifested as an extension of G2 phase. At 72 h, a significant shortening of the G1 phase means that cells enter the DNA replication phase faster from the growth phase, a significant extension of the S phase means that the DNA replication process requires more time, as electrical stimulation affects the activity of DNA replication related enzymes or the function of DNA polymerase, resulting in a prolonged replication process. A slight extension of the G2 phase indicates that cells need more time to check the integrity of DNA replication and prepare for cell division before entering mitosis, which is related to the regulation of cell cycle checkpoints by electrical stimulation. The change in cycle indicates an accelerated rate of cell proliferation, but the mechanism behind it still requires more biological experiments to investigate in future work. The subsequent cell proliferation and scratch experiments confirmed this theory, shown in Fig. 3b (MTT) and Fig. 3c, under electrical stimulation, the proliferation rate of PC12 neurons cells was significantly higher than that of the control group [43,44].

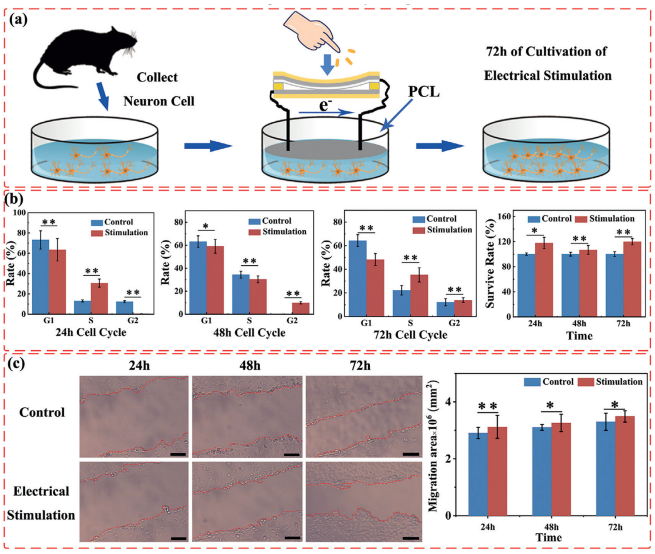


Fig. 3. *In vitro* study on the proliferation properties of triboelectric nanogenerator. (a) The schematic representing the influence of triboelectric nanogenerator on PC12 cell. (b) The ratio of cells in G1, S and G2 phases of cell cycle during 72 h of electrical simulation medium and normal medium. (c) Microscopic images of nerve cell during the scratch migration assay. PC12 cell was cultured in DMEM with or without electrical stimulation. Scale bar: 20 μm. Data are expressed as mean values ± standard deviation (S.D) ($n = 4$, $^{*}P < 0.05$, $^{**}P < 0.01$).

The schematic diagram of neural repair in rats is shown in Fig. 4a. Due to the fact that the sciatic nerve is larger and more convenient to operate compared to other nerves, the commonly used experimental model for peripheral nerve regeneration in clinical practice is sciatic nerve injury [45–47]. The most commonly used method is sciatic nerve injury caused by clamping [48]. Fig. 4b shows the experiment of electrical stimulation of the sciatic nerve in rats. During the first test, rats were anaesthetized and tested with an external pressure device to check whether the piezoelectricity worked normally. Under a force of 1 N, TENG generated approximately 0.12 V alternating voltage, indicating that the friction power generation device is working well and can continuously and stably generate electricity. Subsequently, TENG can be placed on the legs of rats to generate electricity and stimulate sciatic nerve repair through rat movement, as shown in Fig. S5 (Supporting information). Figs. 4c and d show the injury of sciatic nerve and PCL wrapped nerve display diagram. It was seen that the original milky sciatic nerve is transparent, indicating that the sciatic nerve has been damaged after clamped. The defect of the sciatic nerve in the rat was gently wrapped with a nerve conduit and used a suture to prevent slippage, and an external triboelectric nanogenerator was connected, as shown in Fig. 4d. The physical parameters of the nerve conduit are shown in supporting information. Here, we mainly observe the healing of mouse Nervous tissue utilizing tissue staining and sectioning. On the first day after surgery, the control group and the treatment group showed a disordered arrangement of nerve fibers, fracture of nerve axons and disintegration of the myelin sheath (Figs. 4e and f), through the observed of hematoxylin-eosin (H&E) staining. In the presented study, we have meticulously enhanced the application scope of frictional nanogenerators within biological matrices. This advancement was achieved by precisely modulating the electrical potential generated

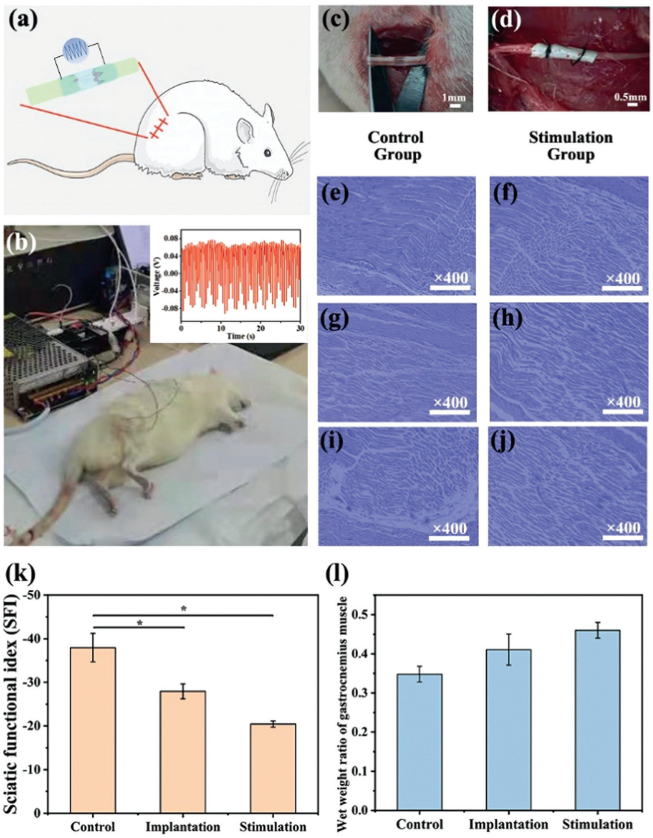


Fig. 4. *In vivo* implantation of triboelectric nanogenerator and functional recovery. (a) Surgical image of sciatic nerve implanted with triboelectric nanogenerator in rats. (b) Apparatus for electric stimulation for rat and stable voltage output. (c) The sciatic nerve is crushed. (d) PCL-Ag was wrapped with PCL-Ag. (e, f) After 1 week, the sciatic nerve section of the control group and the experience group ($n = 6$). (g, h) After 2 weeks, the sciatic nerve section of the control group and the experience group ($n = 6$). (i, j) After 4 weeks, the sciatic nerve section of the control group and the experience group ($n = 6$). (k) SFI measurements of control, stimulation group treatment for 4 weeks ($n = 6$). (l) The wet weight of gastrocnemius muscle of control, stimulation group treatment for 4 weeks. Data are expressed as mean values ± S.D. ($n = 6$, $^*P < 0.05$).

by PDMS, integrated with a meticulously calibrated ratio of mesoporous silica. The myelin sheath's orderly structure, as observed in Figs. 4g and h, was notably more organized compared to the untreated nerve tissue, which is indicative of a heightened state of cellular organization post-electrical stimulation therapy.

Following a period of electrical stimulation therapy spanning four weeks, a significant increase in neuronal density within the treatment group was recorded, as illustrated in Fig. 4j. In stark contrast, the absence of neuronal presence in the unstimulated sciatic nerve tissue, as depicted in Fig. 4i, underscores the pivotal role of electrical stimulation in neuronal development. Concurrently, a substantial increase in the population of Schwann cells was detected, signifying an active phase of nerve tissue regeneration. However, the tissue's disorganized state, as shown in Figs. 4e and f, suggests that while growth is occurring, the structural integrity of the nerve tissue is yet to be fully realized.

Upon reaching the four-week mark, the myelin sheath structure of the unstimulated nerve tissue had begun to form, albeit with a still-disordered neuronal arrangement, as observed in Fig. 4g. Comparatively, the treatment group exhibited a pronounced enhancement in both neuronal density and axonal length after the same duration. These observations collectively suggest that, encased within conductive conduits, electrical stimulation serves as an efficacious modality to foster the regeneration of nerve conduits, thereby facilitating the restoration of nerve tissue integrity.

For the purpose of a more precise evaluation of sciatic nerve regeneration in a rat SNI model, an analysis of the sciatic function index (SFI) was performed, as depicted in Fig. 4k. The SFI is a quantitative metric where an optimal value approaching zero indicates a superior restoration of nerve functionally [49,50]. The experimental finding suggest that rats subjected to electrical stimulation, which using triboelectrification character of triboelectric nanogenerators exhibit accelerated sciatic nerve recovery and enhanced functional restoration. In addition, after euthanizing the rats, the gastrocnemius muscles of both legs were obtained for wet weight comparison, and the muscle weight serves as a proxy for the degree of muscle atrophy associated with nerve damage [46,51]. Fig. 4l illustrates that the gastrocnemius muscle atrophy in the electrically stimulated group is less pronounced compared control group and implant group. these observations infer that electrical stimulation may facilitate an augmented nerve repair process and reduce muscle atrophy. The specific morphology of the gastrocnemius muscle is shown in Fig. S6 (Supporting information). The above animal experiments have demonstrated that self-powering animals can promote rapid repair of the sciatic nerve, prevent gastrocnemius muscle atrophy, and further prove that electrical stimulation is beneficial for accelerating nerve repair. The repaired mechanism by which TENGs may be related to the influx of Ca^{2+} [52]. Under the mediation of Ca^{2+}, the upregulation of BDNF occurs, which increases the expression of regeneration-associated genes (RAGs), T-$\alpha-1$ tubulin, and GAP-43 through the cyclic adenosine monophosphate (cAMP) pathway, thereby promoting neuronal generation [53,54]. Additionally, in terms of electrical stimulation, it can promote the transition of macrophages from the M1 phenotype to the M2 phenotype, effectively clearing myelin debris and alleviating local inflammatory responses, accelerating nerve repair [55].

In this study, we developed a neural repair device that includes a frictional electric nanogenerator device and a neural conduit. Using of mesoporous silica ensures the structural stability and charge stability of the device. In the device, content of mesoporous H-SiO_2 is 5%, and the ratio of PDMS monomer to curing agent is 10:1. The design not only ensure the mechanical properties of the material, but also effectively guarantee the charge collection of the TENG. From cell cycle dynamics studies, it was found that electrical stimulation can accelerate the rate of cell proliferation. This discovery was validated in subsequent scratch experiments and cell proliferation experiments. In animal experiments, we used PCL-Ag catheters to effectively apply electrical stimulation to the sciatic nerve. After one month of treatment, the sciatic nerve repair effect of the electrical stimulation group was better than that of the control group, and the nerve fibers were more intact in the tissue sections. In the device, silicon dioxide molecular sieve not only plays a role in stress enhancement, but more importantly, its charge collection function stabilizes the endogenous neural electric field in nerve injury, ensures the maintenance of resting membrane potential, and guarantees the consistency of electrical stimulation level. In summary, this report introduces a flexible piezoelectric device that can repair nerve tissue through endogenous mechanical stimulation and has broad application prospects.

Declaration of competing interest

The authors declare that they have no known competing financial interests or personal relationships that could have appeared to influence the work reported in this paper.

CRediT authorship contribution statement

Chenglong Cai: Writing – original draft. **Ting Wang:** Writing – review & editing. **Yixin Zhang:** Data curation. **Conghao Lin:** Formal

analysis. **Zhangqi Feng:** Resources. **Yan Cai:** Software. **Nongyue He:** Resources.

Acknowledgments

We thank for the funding supports from Scene Ray. This research is supported by the Natural Science Foundation of China (No. 11204033), CMA L'Oreal China Skin Grant 2015 (No. S2015121421) and the Open Research Fund of State Key Laboratory of Natural Medicines, China Pharmaceutical University (No. SKLN-MKF201803), Southeast University Institution Basal Research Fund.

Supplementary materials

Supplementary material associated with this article can be found, in the online version, at doi:10.1016/j.cclet.2025.111087.

References

[1] M.C. Costello, E.L. Errante, T. Smartz, et al., Front. Neurosci. 17 (2023) 1162851.
[2] M.C. Yoo, J.H. Kim, Y.J. Kim, et al., J. Clin. Med. 12 (2023) 4133.
[3] R. Javed, Q. Ao, J. Neurorestoratol. 10 (2022) 1–12.
[4] K. Haastert-Talini, R. Schmitte, N. Korte, et al., J. Neurotraum. 28 (2011) 661–674.
[5] N.T. Morrell, R.K. Dahlberg, K.L. Scott, J. Am. Acad. Orthop. Sur. 32 (2024) 156–161.
[6] K.J. Zuo, T. Gordon, K.M. Chan, et al., Exp. Neurol. 332 (2020) 113397.
[7] A. Lin, E. Shaaya, J.S. Calvert, et al., Neurospine 19 (2022) 703–734.
[8] J.Y. Wang, Y. Yuan, S.Y. Zhang, et al., Adv. Sci. 11 (2024) 2302988.
[9] J. Gu, C. Wu, X. He, et al., ACS Biomater. Sci. Eng. 9 (2023) 2615–2624.
[10] A.A. Al-Majed, C.M. Neumann, T.M. Brushart, et al., J. Neurosci. 20 (2000) 2602–2608.
[11] B.Q. Lai, R.J. Wu, W.T. Han, et al., Biomaterials 297 (2023) 122103.
[12] Y.B. Feng, Z.Y. Yu, H. Liu, et al., Mater. Today 71 (2023) 50–62.
[13] C.W. Hu, B. Liu, X.Y. Huang, et al., ACS Nano 18 (2024) 14427–14440.
[14] E. Asensio-Pinilla, E. Udina, J. Jaramillo, et al., Exp. Neurol. 219 (2009) 258–265.
[15] C.K. Franz, R. Urs, V.F. Rafuse, Brain 6 (2008) 1492–1505.
[16] A.W. English, G. Schwartz, W. Meador, et al., Dev. Neurobiol. 67 (2010) 158–172.
[17] Q. Li, B. Kang, L. Wang, et al., Chin. Chem. Lett. 33 (2022) 1308–1312.
[18] T. Gordon, N. Amirjani, D.C. Edwards, et al., Exp. Neurol. 223 (2010) 192–202.
[19] Y. Zhang, C. Xue, Y. Zhang, et al., Chin. Chem. Lett. 35 (2024) 109169.
[20] M. Fallahrad, A.L. Zannou, N. Khadka, et al., J. Physiol. 597 (2019) 2131–2137.
[21] J.B. Hjukse, M.F.D.L. Puebla, G.F. Vindedal, et al., Glia 71 (2023) 2770–2781.
[22] F.G. Roca, S.S. Requena, M.M. Pradas, et al., Int. J. Mol. Sci. 23 (2022) 6362.
[23] Y. Sun, Z. Xiao, B. Chen, et al., Adv. Mater. 26 (2024) 2400346.
[24] J.Q. Liu, H. Liu, D.X. Xu, et al., Biosens. Bioelectron. 209 (2022) 114252.
[25] W. Zhong, L. Xu, H. Wang, et al., Adv. Funct. Mater. 29 (2019) 1905319.
[26] M. Sahoo, S. Lai, J. Wu, et al., Nanomaterials 11 (2021) 2276.
[27] X.T. Yan, Y.K. Jin, X.M. Chen, et al., Sci. China Phys. Mech. 63 (2020) 224601.
[28] B. Sun, G.D. Zhou, K. Xu, et al., ACS Mater. Lett. 2 (2020) 1669–1690.
[29] P.G. Pai, S.S. Chao, Y. Takagi, et al., J. Vac. Sci. Technol. A 4 (1986) 689–694.
[30] R.M. Almeida, C.G. Pantano, J. Appl. Phys. 68 (1990) 4225–4232.
[31] C.T. Kirk, Phys. Rev. B 38 (1988) 1255–1273.
[32] R.M. Almeida, Phys. Rev. B 53 (1996) 14656–14658.
[33] G.M. Kim, S.J. Lee, C.L. Kim, Materials 14 (2021) 4489.
[34] W.S. Lee, K.S. Yeo, A. Andriyana, et al., Mater. Des. 96 (2016) 470–475.
[35] A.R. Wheeler, G. Trapp, O. Trapp, R.N. Zare, Electrophoresis 25 (2004) 1120–1124.
[36] W. Li, Y. Xiang, W. Zhang, et al., Nano Energy 113 (2023) 108539.
[37] T. Huang, H. Yu, H. Wang, et al., J. Phys. Chem. C 120 (2016) 26600–26608.
[38] V. Nguyen, R. Yang, Nano Energy 2 (2013) 604–608.
[39] J. Chen, H. Guo, X. He, et al., ACS Appl. Mater. Interfaces 8 (2016) 736–744.
[40] M. He, W. Du, Y. Feng, et al., Nano Energy 86 (2021) 106058.
[41] Z. Liu, X. Wan, Z.L. Wang, L. Li, Adv. Mater. 33 (2021) 2007429.
[42] Q. Zheng, Y. Zou, Y. Zhang, et al., Sci. Adv. 2 (2016) e1501478.
[43] Y. Li, T. Dong, Z. Li, et al., Mater. Today Chem. 24 (2022) 100944.
[44] L. Liu, D. Tian, C. Liu, et al., Med. Sci. Monitor. 25 (2019) 10067–10076.
[45] E. Ogut, F.B. Yildirim, L. Sarikcioglu, et al., Kurume Med. J. 65 (2020) 137–144.
[46] L. Zeng, Y. Cen, J. Chen, et al., Acupunct. Med. 38 (2020) 181–187.
[47] S. Knorr, L. Rauschenberger, T. Lang, et al., J. Vis. Exp. 173 (2021) e62606.
[48] Z. Yang, Y. Yang, Y.C. Xu, et al., Stem Cell Res. Ther. 12 (2021) 442.
[49] M.H. Hong, H.J. Hong, H. Pang, et al., ACS Biomater. Sci. Eng. 4 (2018) 576–586.
[50] X.M. Sun, W. Wang, Y.Y. Dong, et al., Iran. J. Basic Med. Sci. 23 (2020) 654–662.
[51] Q.Q. Niu, J.J. Shen, W.H. Liang, et al., Biomaterials 318 (2025) 123185.
[52] E.P. Knott, M. Assi, D.D. Pearse, Biomed. Res. Int. 2014 (2014) 651625.
[53] V. Brügger, M. Duman, M. Bochud, et al., Nat. Commun. 8 (2017) 14272.
[54] N. Li, X.M. Zhang, Q. Song, et al., Biomaterials 32 (2011) 9374–9382.
[55] N.A. Mclean, V.M.K. Verg, Glia 64 (2016) 1546–1561.